

Localization and capacitance fluctuations in disordered Au nanojunctions

M. Bowman, A. Anaya, A. L. Korotkov, and D. Davidović
Georgia Institute of Technology, Atlanta, Georgia 30332, USA

(Received 10 November 2003; revised manuscript received 5 February 2004; published 18 May 2004)

Nanojunctions, containing atomic-scale gold contacts between strongly disordered leads, exhibit different transport properties at room temperature and at low temperature. At room temperature, the nanojunctions exhibit conductance quantization effects. At low temperatures, the contacts exhibit Coulomb blockade. We show that the differences between the room-temperature and low-temperature properties arise from the localization of electronic states in the leads. The charging energy and capacitance of the nanojunctions exhibit strong fluctuations, with applied magnetic field at low temperature, as predicted theoretically.

DOI: 10.1103/PhysRevB.69.205405

PACS number(s): 73.23.-b, 73.63.-b, 73.21.-b

I. INTRODUCTION

The prospect of molecular electronics as a potential alternative to conventional silicon-based electronics has led to an increased interest in fabrication of atomic-scale gaps and atomic-scale contacts between metallic electrodes. Examples include atomic-scale gaps formed by mechanically controlled break junctions,¹⁻⁶ electrodeposition,⁷⁻¹¹ and electromigration.¹²⁻¹⁴ In these fabrication techniques, one can determine whether a junction has atomic-scale dimensions by changing the conductance of the junction around the conductance quantum $G_0 = e^2/h$. Discrete steps in conductance of order G_0 indicate that the contacts have atomic-scale dimensions. This scheme works remarkably well in cases where the gaps and the contacts are formed in ultrahigh-vacuum (UHV) conditions, such as mechanically controlled break junctions at cryogenic temperatures.¹⁵

Some schemes for generating atomic-scale gaps involve exposure of these gaps to non-UHV environment, such as air^{12,14} or ionic solutions.⁷⁻¹¹ In this case, intermixing between atoms in the leads and impurity molecules (such as H₂O) can degrade the quality of the gaps. Understanding of electrical conduction in such disordered atomic-scale gaps and atomic-scale contacts is still lacking.

Recently, Yu and Natelson have studied Au nanojunctions formed by electroplating from an aqueous solution.^{10,11} Transport measurements were carried out at both room temperature and cryogenic temperatures. The authors found different transport properties at room and low temperatures. At room temperature, as the gap size between two Au leads is reduced by electroplating, conductance increased in discrete steps of order G_0 , suggesting that the contacts were atomic scale, consistent with the prior work.⁷⁻⁹ In addition, the nanojunctions were Ohmic at room temperature.

At $T = 1.8$ K, however, Au junctions with room-temperature conductance $G(300\text{ K}) \sim G_0$, the conductance at zero-bias voltage and $T = 1.8$ K was suppressed by $\approx 100\%$, which was referred to as the zero-bias anomaly (ZBA). They argued that ZBA's displayed a suppression of the density of states in the leads at the Fermi level, as a result of disorder introduced by the electroplating process. The disorder was attributed to the grain boundaries and adsorption of impurities from the solution.

We have reported similar observations in Au nanojunctions

formed by an electric-field-induced migration process.¹⁴ At room temperature, as the conductance of the junctions increased from a value below the conductance quantum to above the conductance quantum, the conductance displayed discrete steps in conductance, of order G_0 . In addition, the room temperature I - V curves of the samples were linear (Ohmic).

At low temperatures, we found strong ZBA's in samples with $G(300\text{ K}) \sim G_0$, similar to the ZBA's in electroplated Au nanojunctions. However, samples with $G(300\text{ K}) < G_0$ were found to exhibit Coulomb blockade, proved by the quasiperiodic gate-voltage dependence of the conductance at $T = 0.015$ K. Coulomb blockade was attributed to single-electron charging effects on one or a few grains in the leads. The data fit exceptionally well the theories of Coulomb blockade in the weak^{16,17} and the strong-coupling regimes.¹⁸

In this paper, we first show that Coulomb blockade in Au nanojunctions is not restricted to single-electron charging on one or few metallic grains. In fact, Coulomb blockade is observed when the resistance of the leads is comparable with the resistance of the contacts, even if there are no apparent grains in the leads. We propose a general model of a disordered Au nanojunction containing atomic-scale contacts, which is sketched in Fig. 1. Reservoirs R_1 and R_2 are bulk Au films, which are good metals. C_1 and C_2 are atomic-scale metallic contacts that are responsible for conductance quantization at room temperature. L_1 and L_2 are highly disordered leads, with room-temperature resistances smaller than

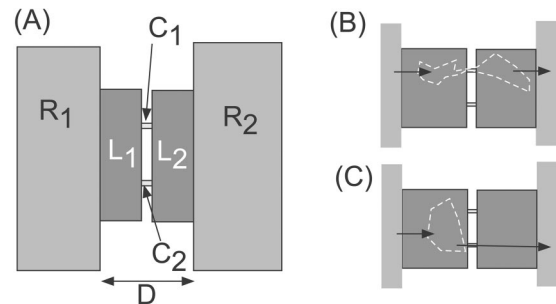


FIG. 1. (a) Disordered Au nanojunction. (b) Sequential electron tunneling through the nanojunction, via a symmetric localized puddle of electrons. (c) Sequential electron tunneling through the nanojunction, via an asymmetric localized puddle of electrons.

or comparable to the resistance of atomic-scale contacts.

The model reconciles the difference between room- and low-temperature transport properties of Au nanojunctions, as follows. The resistivity of the leads is assumed high enough to cause strong localization. However, the characteristic temperature at which localization suppresses conductivity in the leads is assumed to be smaller than 300 K. In this case, the resistance of the contacts dominates at room temperature, explaining conductance quantization and Ohmic properties. At low temperatures, however, the resistance of the leads becomes much larger than the resistance of the atomic-scale contacts, explaining Coulomb blockade and ZBA's. This interpretation of ZBA's in terms of localization is different from the alternative interpretation in terms of suppression of the density of states in the leads.^{10,11} In Sec. V we explain the difference in more detail.

After our model is presented, we discuss capacitance fluctuations of the nanojunctions with applied magnetic field. The capacitance fluctuations in coherent conductors in the charging regime have been predicted theoretically,¹⁹ but have not yet been demonstrated experimentally. The strong disorder combined with the small size of our nanojunctions makes it possible to study charging effects in the phase-coherent regime, permitting us to demonstrate and explore capacitance fluctuations.

The paper is organized as follows. In Sec. II we give a detailed summary of the nanojunction fabrication process and arrive at the nanojunction model shown in Fig. 1(a). In Sec. III we present Coulomb-blockade measurements and discuss electron localization in the leads. In Sec. IV we discuss capacitance fluctuations. In Sec. V we explain the differences between our samples and electroplated nanojunctions.

II. FABRICATION OF GOLD NANOJUNCTIONS

The fabrication of Au nanojunctions used in this paper has been described in Refs. 14 and 20. In this section we summarize the fabrication process. We present data and images of the nanojunctions, which have improved our understanding of nanojunction properties since prior publications.

To create a nanojunction between two Au films, we deposit Au atoms over a 70 nm wide slit, as shown in Fig. 2(a). The slit is created in Si_3N_4 using electron-beam lithography and etching.¹⁴ The large undercut serves to prevent the connection between two Au films. The exposed length of the slit is 0.1 mm. The current between the films is monitored *in situ*. The current limiting resistor R_S is added in series with the sample.

Gold deposition is done by thermal evaporation and the deposition rate is 2.5 Å/s. The background pressure of the deposition chamber measured near the gate valve of the pump is $\sim 10^{-7}$ Torr. Because water molecules outgas from the mask and other nearby surfaces, the sample pressure is higher. The pressure measured with a gauge placed near the sample is in the 10^{-6} Torr range.

During the deposition, the gap between two gold films is reduced in proportion to the film thickness. If the bias voltage is weak (< 0.1 V), then the two gold films electrically

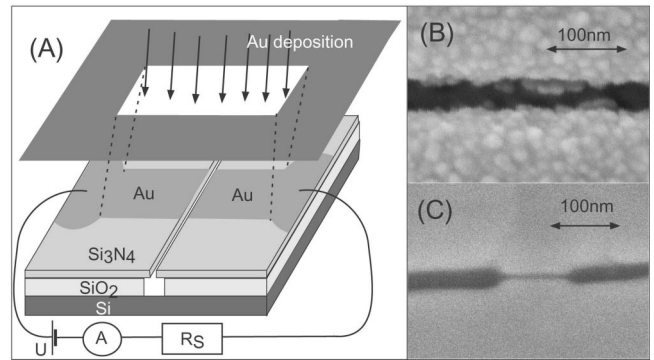


FIG. 2. (a) Deposition of Au over a 70 nm wide slit. (b) Image of the gap between two 70 nm thick Au films grown at low bias voltage. (c) Image of the gap between two 70 nm thick Au films grown at high bias voltage.

connect when the thickness of the film reaches about 70 nm. Figure 2(b) shows the shape of the gap between two Au films of thickness 70 nm grown at $U = 0.1$ V. The films are not connected in this sample. The edge of the film is quite rough because of grains sticking to the edge of the gap. At 70 nm thickness, there is a $\sim 50\%$ chance that there is a pair of grains attached on the opposite sides of the gap and that are in electric contact. By stopping the deposition at the moment when the desired current is detected, we create an atomic-scale gap or an atomic-scale contact.

A. Electric-field-induced surface diffusion

The bias voltage has a strong influence on the shape and electric properties of the nanojunctions. In general, polarization effects from the applied electric field can induce atom migration processes with a “hierarchy of activation energies.”²¹ These processes include electric-field induced surface diffusion, migration due to localized heating, elastic and plastic deformation, and field desorption. The activation energy of these processes depends on both the electric field and the electric-field gradient. It has been demonstrated that surface atom diffusion caused by the field gradient has the lowest activation energy.²¹

In our samples, if the voltage applied between the films is large (~ 10 V), a strong electric field inside the gap can pull a pair of protrusions from the opposing sides of the gap. Figure 2(c) shows the shape of the gap between two Au films grown at 20 V. The edges of the films are much smoother than those in Fig. 2(b). In addition, the film, in the vicinity of the gap in Fig. 2(c), is also much smoother than the film in Fig. 2(b).

These differences can be explained by field induced surface diffusion. At large bias voltage, roughness along the film edges [Fig. 2(b)] induces field gradients, decreasing the activation energy for surface diffusion. In response, surface Au atoms diffuse where the electric-field gradient is the strongest, thereby reducing surface roughness.

In the sample in Fig. 2(c), there is neither mechanical nor electric contact between the two films. This shows that the

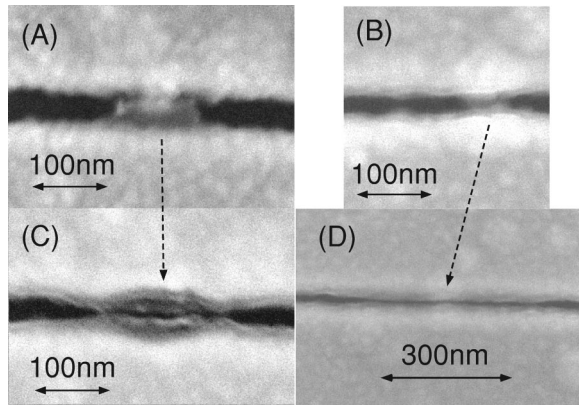


FIG. 3. (a) and (b) Two tunneling junctions formed at 10 V bias voltage. (c) and (d) The same contacts, after the conductance is increased above $2e^2/h$.

protrusion stopped growing on its own, before a contact could have been established. The two protrusions are almost mirror images of each other.

Processes such as elastic and plastic deformation and field desorption are driven by the magnitude of the electric field, not the field gradient, and therefore cannot be responsible for protrusion growth. The electric field in Fig. 2(c) is strongest where the gap is smallest, which would increase the speed of the protrusion growth due to elastic or plastic deformation. On the other hand, the electric-field gradient is weak inside this region, thereby decreasing the speed of protrusion growth due to surface diffusion.

B. Tunneling contacts

For most of our samples, the electric-field induced surface diffusion leads to a contact between the two protrusions. Figures 3(a) and 3(b) show two such contacts, formed during growth at 10 V. Deposition of Au was stopped as soon as the slightest electric contact was detected. The electric contact was exposed to 10 V for ≈ 1 s, and then the bias voltage was quickly reduced to zero (at a rate of 1 V in 10 ms). I - V curves were obtained by measuring current while bias voltage was reduced to zero. The samples were subsequently transferred to the scanning electron microscope (SEM) and images were taken.

The resistance of the junctions is large compared to the resistance quantum. The I - V curves fit quite well the model of field emission through a tunneling barrier with a barrier height close to the work function of Au (5.1 eV) and the barrier thickness of about 10 Å, as shown in Fig. 4(a). The fitting is described in Ref. 20.

The key point that we want to make here is that the voltage drop of 10 V is not distributed uniformly through the leads. It is localized within a single tunneling junction. If it were otherwise, the I - V curve would exhibit less barrier bending than that in Fig. 4(a). For example, assume that there are two tunneling junctions with the same resistance and barrier height, connected in series. In this case, the voltage drop across each of the junctions would be one-half of the applied voltage, thus fitting to the I - V curve of a tunnel-

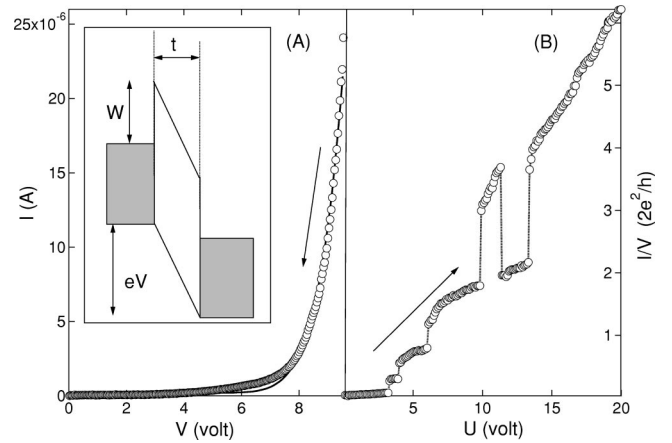


FIG. 4. (a) Circles: I - V curve of a Au nanojunction. Line: fit to the field-emission model. Inset: Schematic of the field-emission model. W is the tunneling barrier height and t is the barrier thickness. The best-fit parameters: $W=5.8$ eV and $t=10.1$ Å. (b) Discrete steps in conductance of order $2e^2/h$ in a current limited Au nanojunction.

ing junction would yield a barrier height which would be twice the work function of Au. The fact that the best-fit parameter for the barrier height is only slightly larger than the work function of Au indicates that the lead resistance is much smaller than the resistance V/I of the junction at 10 V bias voltage, e.g., $R_{lead} \ll 250$ k Ω or $G_{lead} \gg 0.1e^2/h$.

It is striking that tunneling contacts survive at 10 V bias voltage, since a conventional tunneling junction with a similar barrier thickness would typically suffer an electric break down at 10 V. We explain the stability of our atomic-scale gaps at 10 V with a dynamical equilibrium between two opposing atom migration processes.²⁰ At 10 V, the surface diffusion is opposed by electromigration (which increases the gap between the two films).

C. Atomic-scale contacts

After reducing the bias voltage quickly to zero as described above, we introduce a serial resistor $R_S=20$ k Ω and start increasing U at a rate of 1 V/s. The serial resistor limits the current flowing through the junction, thereby limiting electromigration. Consequently, the conductance can exceed e^2/h .

At a bias voltage of $U \sim 4$ V, conductance of the device begins to increase in discrete steps as a function of U .¹⁴ An example is shown in Fig. 4(b). The step size is of order $(0.2-2)e^2/h$, suggesting that the junction contains atomic-scale contacts. We have recently, confirmed these discrete conductance steps at series resistance $R_S=100$ k Ω , showing that the conductance steps are intrinsic to the junction and not biased by our choice of R_S .

In addition to these discrete steps, the conductance changes continuously as a function of U , suggesting that there is a distributed contribution to the resistance of the junction, from the leads. In Figs. 3(c) and 3(d) we show the junctions from Figs. 3(a) and 3(d), respectively, while inside the SEM, after the conductance was increased to $\approx 2e^2/h$

and $\approx 6e^2/h$, respectively. One notices that the length of the junctions increases with conductance. We observe that the conductance is roughly proportional to the length. The conductance per unit length is $G/L \approx 600$ S/m. Among different samples, G/L fluctuates by about a factor of 2.

Thus, the increase in G arises from the addition of Au into the nanojunction. Notice that the gap in the junction in Fig. 3(d) remains well defined. We thus arrive at a model for the nanojunction sketched in Fig. 1(a). Reservoirs R_1 and R_2 are bulk Au films, which are good conductors with sheet resistance of $\approx 5 \Omega$. C_1 and C_2 are atomic-scale contacts responsible for conductance quantization. Finally, L_1 and L_2 are the disordered leads generated by the atom migration processes. From the images in Fig. 3, we obtain that the size of the leads [D in Fig. 1(a)] is ≈ 50 nm.

Using Ohm's laws, the conductance of the junction can be written as

$$G = \sum_i \frac{1}{1/G^i + 1/G_{L_1}^i + 1/G_{L_2}^i}, \quad (1)$$

where G^i refers to the conductance of an atomic-scale contact in the gap, and $G_{L_{1,2}}^i$ are the conductances between the contacts and the reservoirs. As the junction dimensions increase, $G_{L_{1,2}}^i$ changes continuously and G^i changes in discrete steps of order e^2/h .

Because the continuous change in G in Fig. 4(b) is comparable to the discrete steps in G , it follows that the lead resistance is comparable with the resistance of the atomic-scale contacts. To obtain the resistivity of the leads, we need to know the cross section of these protrusions. Unfortunately we cannot obtain this information through SEM imaging. If we assume that the cross section of the protrusion has the thickness of 50 nm, which is comparable to the film thickness, we obtain $\rho \approx 1.7 \times 10^5 \mu\Omega \text{ cm}$.

The resistivity is much larger than the maximum metallic resistivity of $\sim 200 \mu\Omega \text{ cm}$,²² which shows that the leads are highly disordered. The disorder is explained by the intermixing of the impurities into the leads and grain boundaries.¹⁴ In the device in Fig. 3(d) (and many other devices), the leads appear completely uniform down to the imaging resolution (3 nm). We still expect the leads to be granular, with grain diameter d smaller than 3 nm, because Au does not form alloys with water (or other impurities such as O_2 and CO_2 that are present at 10^{-6} Torr background pressure).

In three-dimensional (3D) granular systems, the resistance between the grains (R_g) and the resistivity are related as $\rho \sim R_g d$ and it is known that granular systems in 3D exhibit a metal-insulator transition as a function of R_g .²³ Theoretically, it has been predicted that the transition occurs at $R_g = R_g^C \sim 19R_Q / \ln(E_C/\delta)$, where E_C is the charging energy of the grain and δ is the level spacing inside the grain.^{24,25} In our case, the grain diameter is less than 3 nm and $\rho \approx 10^5 \mu\Omega \text{ cm}$, and we estimate $R_g > 12h/e^2$ and $R_g^C \sim 5h/e^2$. Thus, we expect that the electronic states in the leads are strongly localized.

If the localization length is smaller than the dimensions of the leads, then the lead resistance at low temperature be-

comes much larger than the resistance of the atomic-scale contacts. The temperature dependence of the resistance becomes significant at temperatures well below 300 K, whereas conductance quantization in Au is easily observed at room temperature. This explains the difference between room-temperature and low-temperature properties of nanojunctions.

III. ZERO-BIAS ANOMALIES AND COULOMB BLOCKADE

Electron-transport measurements at low temperatures were carried out using a dilution refrigerator with a base temperature of 0.015 K. The bias voltage, applied to the sample, was the sum of a dc voltage V and an ac voltage with peak-to-peak amplitude $< 10 \mu\text{V}$ and frequency < 100 Hz. A current amplifier measured the current, while lock-in detection from the amplifier output obtained the differential conductance.

The devices were shielded by a Faraday cage which was mounted at the end of the tailpiece of the mixing chamber. The leads were filtered by homemade radiation filters, which were mounted on top of the mixing chamber. The conductance of our devices varies significantly when the temperature of the mixing chamber is reduced from 0.2 K to 0.1 K, see Fig. 8. This dependence weakens (but does not disappear) when the temperature is reduced below 0.05 K, suggesting that the base electronic temperature is about 0.05 K.

Transport properties of our junctions changed dramatically when the temperature was reduced from 300 K to 0.015 K. At 300 K, the junctions were Ohmic and displayed conductance quantization effects. At low temperatures, however, the junctions showed significant suppression near zero-bias voltage.

Devices with $G(300 \text{ K}) < e^2/h$ display Coulomb blockade at $T = 0.015$ K. The Coulomb blockade has been attributed to single-electron charging effects in the grains inside the leads.¹⁴

Devices with $G(300 \text{ K}) > 2e^2/h$ do not display Coulomb blockade at 0.015 K. Instead, the conductance versus voltage at $T = 0.015$ K displays a ZBA. The ZBA's were interpreted as the Coulomb-blockade effect in the strong tunneling regime.¹⁴

A. Microscopic origin of the charging effects and ZBA's

We have found that the Coulomb blockade in our Au junctions is not restricted to single-electron charging effects in the grains in the leads. In fact, the necessary condition to observe Coulomb blockade in our devices is that the leads be highly resistive, regardless of whether the disorder in the leads is granular or homogeneous. For example, if we compare Figs. 3(c) and 3(d), we observe that the leads of the nanojunction in Fig. 3(c) have well distinguished grains, whereas the leads of the nanojunction in Fig. 3(d) are completely uniform. Despite these differences, the I - V curves of these samples at $T = 0.015$ K are very similar.

We are led to the conclusion that the Coulomb blockade and ZBA's at low temperature arise from localization of elec-

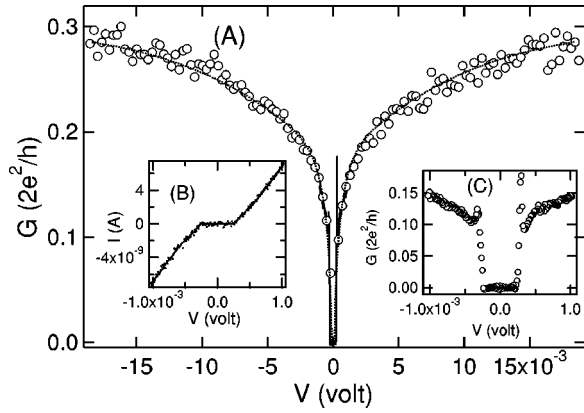


FIG. 5. (a) Differential conductance vs bias voltage of a Au nanojunction at $T=0.015$ K. (b) Current vs voltage at $T=0.015$ K of the nanojunction in a narrow voltage range. (c) Differential conductance vs voltage of the nanojunction at $T=0.015$ K in a narrow voltage range.

tronic states in the leads, which could either be due to localization of electrons within one or a few grains [Fig. 3(c)], or due to localization over a region containing a large number of grains that are too small to observe by the SEM [Fig. 3(d)]. In the Coulomb-blockade regime, electron transport is sequential and takes place via a puddle of electrons in the leads, which is sketched in Figs. 1(b) and 1(c). In Sec. IV, we arrive to the conclusion that the size of the puddle of electrons is comparable to the dimensions of the leads.

Coulomb blockade in distributed systems has been studied in disordered InO_x mesoscopic wires.²⁶ Transport properties of these wires exhibited single-electron charging effects at low temperature, very similar to those in single-electron transistors (SET). However, these wires had no apparent tunneling barriers. The single-electron charging effects were observed if the localization length had been smaller than the sample size. It was suggested that the size of the puddles was comparable to the localization length, but it remained unclear what the junctions were and what formed the puddles of electrons.

B. Effective charging energy

Among devices, the charging energy rapidly decreases as a function of $G(300\text{ K})$. Figure 5(a) shows the conductance versus bias voltage at $T=0.015$ K in a device with $G(300\text{ K})=0.7e^2/h$. This device belongs to a group of borderline devices in which the Coulomb blockade is just resolved at $T=0.015$ K.

The borderline devices are characterized by two voltage scales. If the voltage range is large, e.g., $[-20\text{ mV}, 20\text{ mV}]$ in Fig. 5(a), the curve resembles ZBA's of high conductance devices. Thus, in this voltage range we fit the curve to the model of electron-tunneling through a single-electron transistor in the strong tunneling regime.¹⁸ This leads to the parameter estimates $C_1+C_2=20.8\text{ aF}$, $R_1=2.7\text{ k}\Omega$, and $R_2=34.3\text{ k}\Omega$, where C_1 and C_2 are the bare capacitances between the puddle and the reservoirs, and R_1 and R_2 are the bare resistances between the puddle and the reservoirs. The

corresponding bare charging energy is $e^2/2(C_1+C_2)=3.8\text{ meV}$. The best fit is shown by the dotted line in Fig. 5(a).

Note that the best-fit resistances R_1 and R_2 are rather asymmetric. We have observed the asymmetry in most of the samples that were studied. In our nanojunctions, the tunnel-barriers form by localization (as in Ref. 26) and one possible explanation of the asymmetry would be that the puddle of electrons forms on one side of the contact, which is sketched in Fig. 1(c). In this case, the tunnel coupling between the puddle and the reservoir on the right would be weakened by the atomic contact, explaining the asymmetry.

The conductance in Fig. 5(a) approaches zero at a nonzero zero-bias voltage. Figure 5(c) zooms in to Fig. 5(a) around zero-bias voltage. The corresponding I - V curve is shown in Fig. 5(b). The gap in the I - V curve represents Coulomb blockade. By fitting the low bias voltage I - V curves to the orthodox theory of single-electron tunneling,^{16,17} we estimate $\tilde{C}_1+\tilde{C}_2=442\text{ aF}$, $\tilde{R}_1=34\text{ k}\Omega$, and $\tilde{R}_2=65\text{ k}\Omega$ for the capacitances and the resistances between the puddle and the reservoirs. The fit is shown by the line in Fig. 5(b). The corresponding charging energy is $\tilde{E}_C=e^2/2(\tilde{C}_1+\tilde{C}_2)=0.18\text{ meV}$, a factor of 21 smaller than the bare charging energy estimated above.

Theoretically, it has been predicted that Coulomb blockade persists in any diffusive conductor, even if the resistances between the conductor and the reservoirs is much larger than the resistance quantum.^{19,27} The persistence of charging effects in a single-electron transistor in strong coupling to the leads has been demonstrated experimentally.^{28,29} It has been predicted that the effective charging energy is given as

$$\tilde{E}_C = E_C e^{-\alpha G/G_0}, \quad (2)$$

where $G=G_1+G_2$ is the sum of the conductances between the conductor and the reservoirs, $G_0=2e^2/h$, and, finally, α is a constant of order 1.^{19,27}

In our samples, E_C and \tilde{E}_C are interpreted as the bare and effective charging energy, respectively. With $\alpha\approx 0.6$, they are in rough agreement with Eq. (2).

IV. CAPACITANCE FLUCTUATIONS

In conventional single-electron transistors, the charging energy is independent of the applied magnetic field. In contrast, we find that the effective charging energy of our nanojunctions exhibits strong magnetic-field dependence.

Figure 6 displays a gray-scale image of the conductance versus bias voltage and the applied magnetic field in the sample with the I - V curves shown in Fig. 5. The magnetic field is parallel to the slit. The threshold voltage for Coulomb blockade (the gap) exhibits a strong nonmonotonic dependence—fluctuations—with the magnetic field. Around the field of 2 T, the gap approaches zero, and around the field of 11 T, the gap is at maximum. The dependence is reproducible when the measurements are repeated. The amplitude of the gap fluctuations is comparable to the average gap.

The characteristic magnetic-field scale of the gap fluctua-

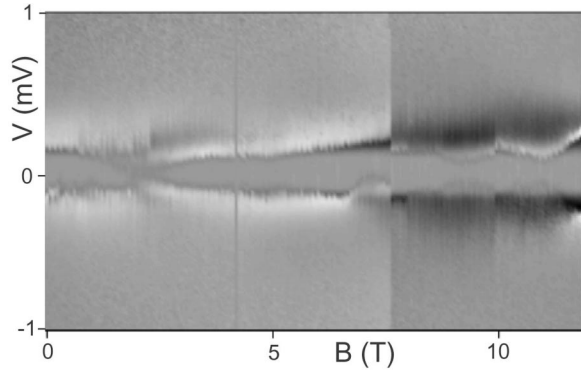


FIG. 6. Conductance (gray) vs magnetic field and bias voltage of the nanojunction at $T=0.015$ K.

tions (B_C) is given by the typical period of the fluctuations. We resolve less than a full period in our magnetic-field range of 12 T, thus $B_C > 12$ T. We have confirmed the gap fluctuations in four additional samples with similar effective charging energies.

We now show that the fluctuations in the gap represent charging energy fluctuations (or capacitance fluctuations). To this end, we examine the gate voltage dependence of the conductance, as a function of the applied magnetic field. Figure 7 displays conductance versus gate voltage and bias voltage at magnetic fields of 0 T, 4 T, 8 T, and 12 T, in a different sample (the previous sample did not have a gate). The fabrication of the gate has been described in Ref. 4.

Figure 7(a) resembles “diamond diagrams” of conductance versus gate voltage and bias voltage of quantum dots.³⁰ The strong dependence of the gap on gate voltage proves that the gap is caused by the Coulomb blockade. In particular, at certain gate voltages, indicated by the groups of four lines that cross at a point along the $V=0$ axis, the gap approaches zero. These points will be referred to as points where the diamonds close, and the conductance at these points will refer to the peak conductance G_{peak} . The valley conductance G_{valley} is defined as the conductance at $V=0$ and at a gate voltage where the gap is at maximum.

There are significant differences between the diamonds in Fig. 7 and the diamonds of conventional single-electron transistors. First, the gate voltage dependence of the gap in Fig.

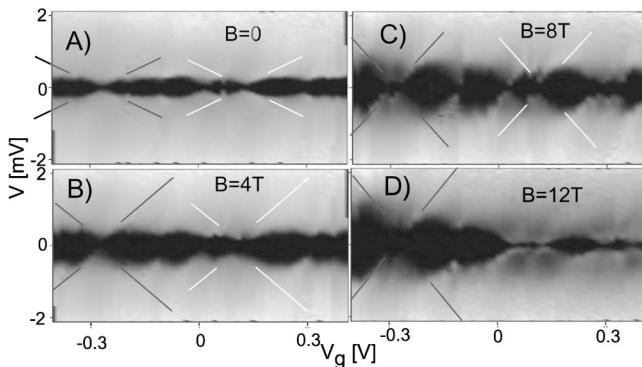


FIG. 7. (a–d) Conductance of a Au nanojunction (gray) vs gate voltage and bias voltage at four magnetic fields at $T=0.015$ K.

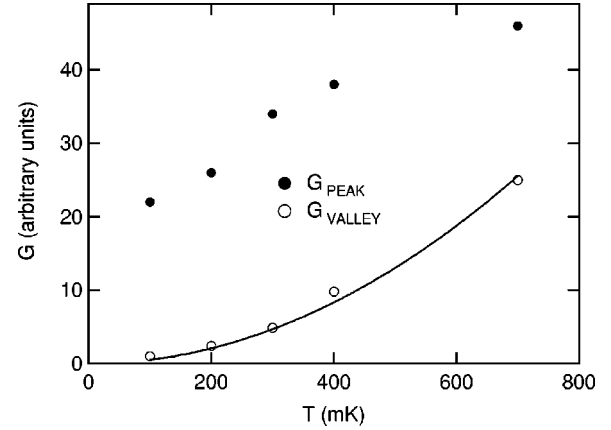


FIG. 8. Temperature dependence of the peak and the valley conductance. The line displays the best fit of the valley conductance to the quadratic temperature dependence.

7 is not periodic. We examined the gate voltage dependence in the range of gate voltages from -2 V to 2, and found that the structure in Fig. 5(a) remained over the extended voltage range. The structure in Fig. 5(a) is quasiperiodic, in that the slopes of the diamond’s edges, near the points where diamonds close, are the same [i.e., the lines in the black and the white groups in Fig. 5(a) have the same slopes].

Discontinuities in conductance, as a function of gate voltage, cause the absence of periodicity in Fig. 7(a). When the gate voltage sweeps are repeated, conductance discontinuities are reproducible, and can be attributed to the shifts in the background charge induced by the changes in gate voltage. The leads are highly disordered, thus they may contain a large number of charge traps in the vicinity of the puddle responsible for Coulomb blockade. The gate voltage can change the state of the charge trap, and causes a discontinuous shift in the background charge.

The second difference between Coulomb blockade in our nanojunctions and that of conventional SET’s is found in the conductance peak’s temperature dependence. Figure 8 shows G_{peak} and G_{valley} versus temperature. G_{peak} decreases significantly with temperature even when $k_B T \ll \tilde{E}_C$. In contrast, with conventional SET’s, G_{peak} has a weak temperature dependence when $k_B T$ is much smaller than the charging energy. It appears that G_{peak} approaches a nonzero value when $T \rightarrow 0$.

At low temperature ($k_B T \ll \tilde{E}_C$), the valley conductance goes to zero as $G_{valley} \sim T^2$, as shown in Fig. 8. The quadratic temperature dependence in the valleys demonstrates that electron transport in the valleys occurs through inelastic cotunneling,³¹ which is possible only if the spacing between energy levels δ in the puddle of electrons is much smaller than $k_B T$. Assuming that the level spacing is given by $\delta \approx 1/[N(0)V]$, where $N(0)$ is the density of states at the Fermi level of Au, and V is the volume of the puddle, we obtain that $V > (10 \text{ nm})^3$. This suggests that the localization length L_s is larger than 10 nm.

At low magnetic fields (≤ 8 T), we can trace the evolution of the diamonds with the magnetic field quite well, despite the discontinuities in the background charge. The points

where diamonds close do not shift with magnetic field in this range. This implies that the capacitance between the puddle and the gate C_g does not vary. Therefore, the geometry of the puddle does not change with magnetic field.

The key effect in Figs. 7(a)–(c) is that it is the puddle’s effective charging energy that changes strongly with magnetic field. From the orthodox theory of Coulomb blockade,¹⁷ the slopes of the lines in Fig. 7 are $\pm eC_g/(2\tilde{C}_1)$ and $\pm eC_g/(2\tilde{C}_2)$, where \tilde{C}_1 and \tilde{C}_2 are the effective capacitances between the puddle and the reservoirs. It follows that \tilde{C}_1 and \tilde{C}_2 fluctuate with field. In particular, from Fig. 7, we obtain $\tilde{C}_1(4\text{ T})=1.8\tilde{C}_1(0)$, $\tilde{C}_1(8\text{ T})=2.3\tilde{C}_1(0)$, and $\tilde{C}_1(12\text{ T})=2.4\tilde{C}_1(0)$.

Nazarov had predicted fluctuations of effective capacitance in coherent conductors in the regime of strong coupling to the reservoirs.¹⁹ With strong coupling, the Coulomb blockade survives in any coherent disordered conductor. In this regime, effective capacitance exhibits mesoscopic fluctuations as a function of the applied magnetic field. These fluctuations are analogous to universal conductance fluctuations.³²

One way to understand capacitance fluctuations is to observe that the effective charging energy, $e^2/2(\tilde{C}_1+\tilde{C}_2)$, exponentially depends on the conductance between the conductor and the reservoirs, see Eq. (2). Then, the universal conductance fluctuations induce fluctuations in G_1+G_2 with field, which leads to the fluctuations in the effective charging energy. Since the amplitude of conductance fluctuations in the diffusive regime is $\sim G_Q$, it follows that the amplitude of the charging energy fluctuations is comparable to the average charging energy, consistent with our data.

We expect that the characteristic magnetic-field scale is given by the flux quantum ($\Phi_0=h/2e$) over the directed area of the puddle, $B_C\sim\Phi_0/L_s^2$, where L_s is roughly the diameter of the puddle (localization length). From $B_C>12\text{ T}$, we obtain $L_s<130\text{ nm}$. Recall that we obtained $L_s>10\text{ nm}$ from the temperature dependence of the valley conductance. Thus, $10\text{ nm}<L_s<130\text{ nm}$ and we conclude that L_s is comparable, within a factor of order 1, to the dimensions of the leads ($D\approx 50\text{ nm}$).

If the magnetic field approaches 12 T, it becomes hard to trace the diamonds. In fact, at the field of 12 T [Fig. 7(d)], the structure is no longer quasiperiodic. The strong-field regime is the subject of current research.

V. COMPARISON WITH ELECTROPLATED NANOSCALE JUNCTIONS

Our introduction described strong ZBA’s, observed in electroplated Au nanoscale junctions containing atomic-scale contacts.^{10,11} The bulk electroplated material was found not to undergo a strong localization transition at low temperatures. In addition, the ZBA’s exhibited scaling with junction size that could not be easily explained in the localization

framework. The scaling suggested that the ZBA’s displayed a suppression in the density of states in the leads.

Note that only if the resistance of atomic-scale contacts is much larger than the lead resistance can the conductance of the contact be proportional to the density of states in the leads, as would be the case in conventional tunneling junctions.³³ Thus, a $\sim 100\%$ suppression of the density of states in electroplated nanoscale junctions must be very local around the atomic-scale contact. If it were otherwise, the conductivity of the leads would be $\sim 100\%$ reduced in a region much larger than the contact size, and the lead resistance would not be much smaller than the resistance of the contact.

In our devices, the localization length is comparable to the dimensions of the leads and the conductance is not proportional to the density of states. The ZBA’s in our nanoscale junctions are caused by the Coulomb blockade on localized puddles of electrons inside the leads, analogous to Coulomb blockade in disordered InO_x wires.²⁶ The ZBA’s are manifestations of Coulomb blockade on these puddles in the regime of strong coupling to the reservoirs.

VI. CONCLUDING REMARKS

Atomic-scale point contacts of Au between strongly disordered leads can have striking differences between their room-temperature and the low-temperature properties. At room temperature the contacts exhibit conductance quantization and are Ohmic, at low temperatures the contacts exhibit Coulomb blockade or zero-bias anomalies. The differences between the room-temperature and the low-temperature properties arise from the localization of electronic states in the leads. The temperature at which the resistance of the leads becomes significantly larger than the resistance of the contacts is much lower than the room temperature.

At low temperature, Coulomb blockade arises from puddles of electrons in the leads that form as a result of localization. One can distinguish between the bare charging energy and the effective charging energy of the puddles. The latter is found to be much smaller than the former, and it exhibits strong fluctuations with an applied magnetic field. The gate voltage effects of a magnetic field demonstrate that the effective capacitance between the puddle and the reservoirs fluctuates with the magnetic field, in agreement with theoretical predictions.

ACKNOWLEDGMENTS

This work was performed in part at the Cornell Nanofabrication Facility, (a member of the National Nanofabrication Users Network), which is supported by the NSF, under Grant No. ECS-9731293, Cornell University and Industrial affiliates, and the Georgia-Tech electron microscopy facility. This research was supported by the David and Lucile Packard Foundation Grant No. 2000-13874 and the NSF Grant No. DMR-0102960.

- ¹J. Moreland and J. W. Ekin, *J. Appl. Phys.* **58**, 3888 (1985).
- ²C. J. Muller, J. M. van Ruitenbeek, and L. J. de Jongh, *Physica C* **191**, 485 (1992).
- ³T. N. Todorov and A. P. Sutton, *Phys. Rev. Lett.* **70**, 2138 (1993).
- ⁴N. Agrait, J. G. Rodrigo, and S. Vieira, *Phys. Rev. B* **47**, 12 345 (1993).
- ⁵L. Olesen, E. Laegsgaard, I. Stensgaard, F. Besenbacher, J. Schiotz, P. Stoltze, K. W. Jacobsen, and J. K. Nørskov, *Phys. Rev. Lett.* **72**, 2251 (1994).
- ⁶S. I. Vedenev, P. Samuely, A. G. M. Yansen, P. Wyder, and V. A. Stepanov, *Physica B* **194**, 1767 (1994).
- ⁷A. F. Morpurgo, C. M. Marcus, and D. B. Robinson, *Appl. Phys. Lett.* **74**, 2084 (1999).
- ⁸C. Z. Li, H. X. He, A. Bogozzi, J. S. Bunch, and N. J. Tao, *Appl. Phys. Lett.* **76**, 1333 (2000).
- ⁹S. Boussaad and N. J. Tao, *Appl. Phys. Lett.* **80**, 2398 (2002).
- ¹⁰L. H. Yu and D. Natelson, *Appl. Phys. Lett.* **82**, 2332 (2003).
- ¹¹L. H. Yu and D. Natelson, *Phys. Rev. B* **68**, 113407 (2003).
- ¹²H. Park, A. K. L. Lim, A. P. Alivisatos, J. Park, and P. L. McEuen, *Appl. Phys. Lett.* **75**, 301 (1999).
- ¹³J. Park *et al.*, *Nature (London)* **417**, 722 (2002).
- ¹⁴A. Anaya, A. L. Korotkov, M. Bowman, J. Waddell, and D. Davidović, *J. Appl. Phys.* **93**, 3501 (2003).
- ¹⁵N. Agrait, A. L. Yeyati, and J. M. V. Ruitenbeek, *Phys. Rep.* **377**, 81 (2003).
- ¹⁶D. V. Averin and A. N. Korotkov, *J. Low Temp. Phys.* **80**, 173 (1990).
- ¹⁷D. V. Averin and K. K. Likharev, in *Mesoscopic Phenomena in Solids*, edited by B. L. Altshuler, P. L. Lee, and R. A. Webb (Elsevier, Amsterdam, 1991), p. 169.
- ¹⁸D. S. Golubev, J. König, H. Schoeller, G. Schön, and A. D. Zaikin, *Phys. Rev. B* **56**, 15 782 (1997).
- ¹⁹Y. V. Nazarov, *Phys. Rev. Lett.* **82**, 1245 (1999).
- ²⁰A. L. Korotkov, M. Bowman, H. J. McGuinness, and D. Davidović, *Nanotechnology* **14**, 42 (2003).
- ²¹T. M. Mayer, J. E. Hueston, G. E. Franklin, A. A. Erchak, and T. A. Michalske, *J. Appl. Phys.* **85**, 8170 (1999).
- ²²Y. Imry, *Introduction to Mesoscopic Physics* (Oxford University Press, New York, 1997).
- ²³K. B. Efetov and A. Tschersich, *Phys. Rev. B* **67**, 174205 (2003).
- ²⁴I. S. Beloborodov, K. B. Efetov, A. Altland, and F. W. J. Hekking, *Phys. Rev. B* **63**, 115109 (2001).
- ²⁵I. S. Beloborodov, K. B. Efetov, A. V. Lopatin, and V. M. Vinokur, *Phys. Rev. Lett.* **91**, 246801 (2003).
- ²⁶V. Chandrasekhar, Z. Ovadyahu, and R. A. Webb, *Phys. Rev. Lett.* **67**, 2862 (1991).
- ²⁷S. V. Panyukov and A. D. Zaikin, *Phys. Rev. Lett.* **67**, 3168 (1991).
- ²⁸D. Chouvaev, L. S. Kuzmin, D. S. Golubev, and A. D. Zaikin, *Phys. Rev. B* **59**, 10 599 (1999).
- ²⁹P. Joyez, V. Bouchiat, D. Esteve, C. Urbina, and M. H. Devoret, *Phys. Rev. Lett.* **79**, 1349 (1997).
- ³⁰L. P. Kouwenhoven, C. Marcus, P. McEuen, S. Tarucha, R. Westervelt, and N. Wingreen, in *Mesoscopic Electron Transport*, edited by L. P. Kouwenhoven, L. L. Sohn, and G. Schön (Elsevier, Amsterdam, 1997), p. 549.
- ³¹D. V. Averin and Y. V. Nazarov (Kluwer Academic, Dordrecht, Plenum Press, New York, 1991).
- ³²S. Washburn and R. A. Webb, *Rep. Prog. Phys.* **55**, 1311 (1992).
- ³³B. L. Altshuler and A. G. Aronov, in *Electron-Electron Interactions in Disordered Systems*, edited by A. L. Efros and M. Pollak (Elsevier, Amsterdam, 1985).